Journal of The Electrochemical Society, **154** (2) B242-B246 (2007)
0013-4651/2006/154(2)/B242/5/$20.00 © The Electrochemical Society

NMR Studies of Mass Transport in High-Acid-Content Fuel Cell Membranes Based on Phosphoric Acid and Polybenzimidazole

J. R. P. Jayakody,[a] S. H. Chung,[b] L. Durantino,[b] H. Zhang,[c] L. Xiao,[c] B. C. Benicewicz,[c,*] and S. G. Greenbaum[a,*,z]

[a]*Department of Physics, Hunter College of the City University of New York, New York, New York 10021, USA*
[b]*Department of Chemistry and Physics, William Paterson University of New Jersey, Wayne, New Jersey 07470, USA*
[c]*Department of Chemistry and Chemical Biology, New York State Center for Polymer Synthesis, Rensselaer Polytechnic Institute, Troy, New York 12180, USA*

Mass-transport studies of phosphoric acid (PA)-doped *meta*-polybenzimidazole (PBI) fuel cell membranes are described. In this study, the fundamental differences in transport properties between *m*-PBI/PA membranes prepared by conventional imbibing procedures and the polyphosphoric acid (PPA) process are explored. The membranes were characterized by proton conductivity and multinuclear (^{1}H and ^{31}P) magnetic resonance measurements. Both short-range and long-range dynamical processes were investigated by spin–lattice and spin–spin relaxation time measurements and by pulsed field gradient diffusion, respectively. Comparative data for pure PA and PPA are included. The high proton conductivity (0.13 S/cm at 160°C) of the PPA-processed membranes is correlated with rapid proton self-diffusion (3×10^{-6} cm^2/s at 180°C). The ^{31}P results reveal the presence of both PA and the dimeric pyrophosphoric acid and indicate strong interaction between the phosphate groups and the *m*-PBI matrix, with negligible anionic transport for both kinds of membranes. The higher concentration of PA in the PPA-processed membranes and differences in membrane morphology may provide an additional proton-transport mechanism involving rapid exchange between the PA and pyrophosphoric acid species.
 [DOI: 10.1149/1.2405726]

Manuscript submitted July 17, 2006; revised manuscript received September 27, 2006.
Available electronically December 27, 2006.

High-temperature polymer electrolyte fuel cell membranes (PEMFCs) operational above 120°C have attracted much interest because they offer many benefits, including increased resistance of fuel impurities, (e.g., carbon monoxide), fast electrode kinetics, and simplified water and thermal management.[1] Among various types of alternative high-temperature membranes developed so far, phosphoric acid (PA)-doped polybenzimidazole (PBI) has been recognized as the most promising candidate for a low-cost and high-performance fuel cell membrane material.[2] It was reported that this polymer electrolyte membrane exhibits high ionic conductivity at temperatures up to 200°C, low gas permeability, excellent oxidative and thermal stability, and a nearly zero water-drag coefficient.[3-5] Briefly, the conventional imbibing method to prepare PA-doped PBI membranes is a multistep process that involves casting the PBI from *N*,*N*-dimethyl acetamide (DMAc) organic solvent and imbibing the PBI film in a PA bath for an extended period of time. Multiple washing and oven drying steps are also needed. This process typically produces PA-doped PBI membranes with a PA doping level of up to 6–10 moles PA per mole of polymer repeat unit (moles PA/PRU). More recently, a novel polyphosphoric acid (PPA) process has been developed that produces PA-doped membranes by employing PPA as both polycondensation reagent to produce high-molecular-weight polymers and casting solvent for film preparation in a one-pot procedure.[6,7] After film casting and exposure to ambient or controlled humidity conditions at room temperature, a transition from sol state to gel state was induced by the hydrolysis of PPA to PA. The resulting novel films retained high levels of phosphoric acid in the gel structure and exhibited high ionic conductivities and stable mechanical properties at elevated temperatures.

Previous nuclear magnetic resonance (NMR) investigations of mass transport in phosphoric acid systems containing water or aprotic solvents have demonstrated that phosphate transport is vehicular, while proton transport occurs via a Grotthus hopping mechanism.[8,9] This conclusion was based on the observed temperature dependence of the product of the diffusion coefficient and the viscosity, which have opposite slopes for ^{1}H and ^{31}P. The most commonly used PEM materials are sulfonated polymers which require a significant amount of water for proton conduction and are consequently limited to operation at temperatures below 100°C.[10] In the context of this investigation, it is noted that the prior work on characterizing the proton transport mechanism has shown that water-molecular diffusion is strongly correlated with proton conductivity.[11,12] It is thus of particular interest to examine proton transport in the absence of water, assess the mobility of the phosphate counterion, and compare the behavior of the PBI/PA membranes prepared by the different processes.

Experimental

Polymer synthesis and membrane fabrication.— Isophthalic acid (9.662 g, 0.0582 mol) (Amoco, 99+%), 3,4,3′,4′-tetraminobiphenyl (TAB) (12.458 g, 0.0582 mol) (Celanese, polymerization grade), and PPA (216.9 g) (FMC Corporation, 115%) were added into a 500 mL, three-neck, round-bottom flask equipped with a nitrogen inlet and overhead stirrer. The monomer concentration was 9.25%. The polymerization mixture was heated from 20 to 195°C in multiple heating steps over 20 h. After polymerization, the solution was very viscous and an additional 27.5 mL of orthophosphoric acid was added to reduce the solution viscosity. After heating at 220°C for 1 h, the solution was cast directly onto glass substrates using a casting blade with a 15 mil gap dimension. The substrates were allowed to stand at room temperature and 25% relative humidity for 3 days. Absorption of water from the environment and subsequent hydrolysis of the PPA to PA induced a sol-to-gel transition that produced 250 μm thick films (referred to as *m*-PBI-ppa) with high acid-doping levels. The polymer inherent viscosity (IV) was 1.49 dL/g.

For conventionally imbibed films (referred to as *m*-PBI-imb), *m*-PBI film cast from DMAc solvent was obtained commercially (Celanese). The polymer IV was measured at 0.89 dL/g. Doping was conducted by submerging the film in 85% PA baths for 24 h at ambient temperature, resulting in 100 μm (wet thickness) films.

Characterization.— PA doping levels were determined by titrating a piece of preweighed membrane with standardized sodium hy-

* Electrochemical Society Active Member.
z E-mail: steve.greenbaum@hunter.cuny.edu

Table I. Properties of *m*-PBI/PA membranes used in this study.

IV[a] (dL/g)	Film process	Film composition: Polymer (wt%)	PA (wt%)	Water (wt%)	PA/PBI (molar ratio)	Conductivity[b] (S/cm)
0.89	Conventionally imbibed	15.6	60.7	23.7	12.2	0.048
1.49	PPA process	14.4	63.3	22.3	13.8	0.13

[a] Determined in concentrated sulfuric acid (96%) at 30.0°C.
[b] Second heating run, after heating to 160°C to remove water. The conductivity was measured at 160°C.

droxide solution. The titrated sample was then washed thoroughly with water and dried in a vacuum oven at 130°C overnight to obtain the dry weight of polymer. The water content of the original film was obtained by subtraction of the titrated PA content and dry-polymer weight from the original film weight. Proton conductivities were measured by a four-point ac impedance method using a Zahner IM6e spectrometer over the frequency range from 1 Hz to 100 kHz at temperatures from 20 to 160°C. The conductivity was calculated by fitting the experimental data with a model of a resistor in parallel with a capacitor. Polymer IVs were measured at a polymer concentration of 0.2 g/dL in concentrated sulfuric acid (96%) at 30.0°C using a Cannon Ubbelohde viscometer.

Initial NMR diffusion measurements were performed on as-synthesized films sealed into 5 mm outer diameter (OD) × 20 mm NMR tubes, in order to ascertain the effect of residual water. However, most of the NMR data were obtained from films that were treated at 150°C in a vacuum oven for 2 h, prior to sealing in NMR tubes. Reference NMR measurements were also made on dry PPA and 100% PA, the latter purchased from Sigma-Aldrich, dried in a vacuum oven at 100°C for 1 h prior to sealing in an NMR tube. NMR measurements were performed on a Chemagnetics CMX-300 spectrometer with ^{1}H Larmor frequency of 301.02 MHz and a ^{31}P frequency of 121.85 MHz. Spectral information and self-diffusion coefficients (D) were obtained. Spectroscopic references were distilled water for ^{1}H and 85% H_3PO_4 for ^{31}P. Spectra were obtained by Fourier transforming the resulting free-induction decay (FID) of single $\pi/2$ pulse sequence. Pulse widths were about 5 μs for ^{31}P and 10 μs for ^{1}H. Self-diffusion coefficients were obtained with a DOTY Z-gradient probe by the NMR pulse gradient spin–echo technique (NMR-PGSE), using the Hahn spin–echo pulse sequence ($\pi/2-\tau-\pi$). For a diffusing system in the presence of a magnetic field the application of square-shaped magnetic gradients of magnitude g and duration δ results in attenuation of the echo amplitude A. This attenuation may be represented by $A(g) = \exp\{-\gamma^2 g^2 D\delta^2[\Delta - (\delta/3)]\}$, where γ, D, and Δ represent the nuclei's gyromagnetic constant, self-diffusion coefficient, and gradient delay. Applied gradient strengths (g) ranged from 0.2 to 1.2 T/m, δ and Δ ranged from about 1.0 to 10 and 5 to 30 ms, respectively. The resulting echo profile vs gradient strength is fitted to the above equation and D is extracted. Uncertainties in self-diffusion coefficient values are ~5%. Spin–spin relaxation (T_2) measurements were obtained using the Hahn spin–echo sequence, and spin–lattice relaxation times (T_1) were evaluated from inversion recovery ($\pi-\tau-\pi/2$) measurements. Variable-temperature NMR measurements were made ranging from ambient to 180°C, with equilibration times of 20–25 min following each temperature change.

Results and Discussion

Although several different PBI chemical structures have been investigated for fuel cell membranes, this study examined the transport properties of the most commonly studied material, *m*-PBI, or poly[2,2′-(1,3-phenylene)-5,5′-bibenzimidazole]. The traditional method to prepare imbibed films (*m*-PBI-imb) involves casting films from organic solvents, followed by solvent evaporation, washing, and drying steps to produce films. Phosphoric acid is imbibed into these films by a subsequent soaking period in phosphoric acid baths. A newer method for preparing acid-doped films involves the synthesis of polymers in PPA and casting films directly from the polymerization solution.[6] Under appropriate conditions, hydrolysis of the PPA to PA induces a sol-to-gel transition that produces membranes (*m*-PBI-ppa) which exhibit properties substantially different than the conventionally imbibed membranes. In this study, membranes produced from the two different processes had similar compositions. The basic characterization data are shown in Table I. For *m*-PBI films, the PA loading levels used in this study were considered high relative to the values reported previously in the literature.

The temperature dependence of the ionic conductivity for both *m*-PBI-imb and *m*-PBI-ppa are displayed in Fig. 1. These curves were recorded after an initial heating run and were reproducible in subsequent runs. The conductivity measured during the first heating was affected by the initial water content, which was removed by evaporation above 100°C during the first heating run. The conductivity of the *m*-PBI-ppa membrane was significantly higher that the *m*-PBI-imb membrane, even at similar PA loading levels.

The effect of residual water can be observed in Fig. 2, which shows NMR ^{1}H diffusion (upper curve) and T_1 (lower curve) results for as-prepared and dried *m*-PBI-ppa membranes. The presence of water clearly augments the proton diffusion compared to that in the dried film through several mechanisms, first through having additional H-bonding sites for the acid proton to transfer between and second, through diffusion of water molecules themselves. The

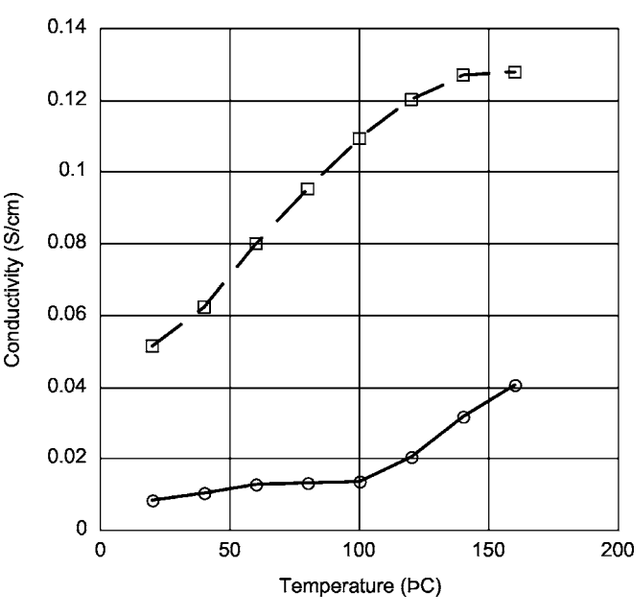

Figure 1. (Upper curve, squares) Ionic conductivities of *m*-PBI-ppa and (lower curve, circles) *m*-PBI-imb films. Both curves were recorded after an initial heating to 160°C to remove residual water.

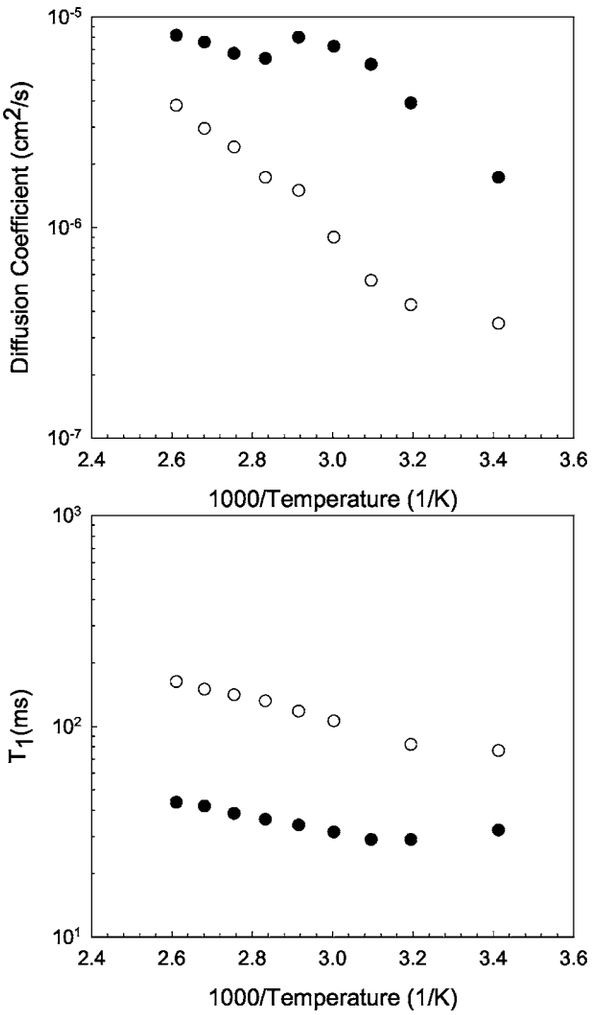

Figure 2. (Upper curve) NMR ^{1}H diffusion and T_1 relaxation results for *m*-PBI-ppa in the (filled circles) as-prepared and (open circles) dried membranes.

abrupt drop in D around 90°C is associated with the removal of water, although it does not fall to the values exhibited by the dried film. Because the sample tubes were sealed, there is some likelihood of residual water remaining in the as-prepared film. The presence of water also affects localized motion as noted in the different T_1 values of the dried and as-prepared films. This effect has also been noted in observing the difference in T_1 between 100% and 85% PA.[8] Proton diffusion results for dried *m*-PBI-ppa, extending to 180°C, are plotted in Fig. 3. For comparison, data for pure PA and PPA are also displayed. It was not possible to measure the proton diffusion coefficient of *m*-PBI-imb due to the short T_2 values characteristic of this material. However, given the highest value of T_2 observed for *m*-PBI-imb, which occurred around 60°C (described more fully below) and the gradient strengths and spacings employed in the PGSE sequence, it is possible to estimate an upper bound for the diffusion coefficient. The result is 10^{-7} cm^2/s and is about 1 order of magnitude lower than in *m*-PBI-ppa. This is consistent with the order-of-magnitude lower conductivity of *m*-PBI-imb relative to *m*-PBI-ppa (Fig. 1). The *m*-PBI-ppa proton diffusion coefficients are in fact much closer to those of PA than PPA, thus providing additional support that the PPA has been completely hydrolyzed into PA and remains as such, even after the water has been driven off. A decrease

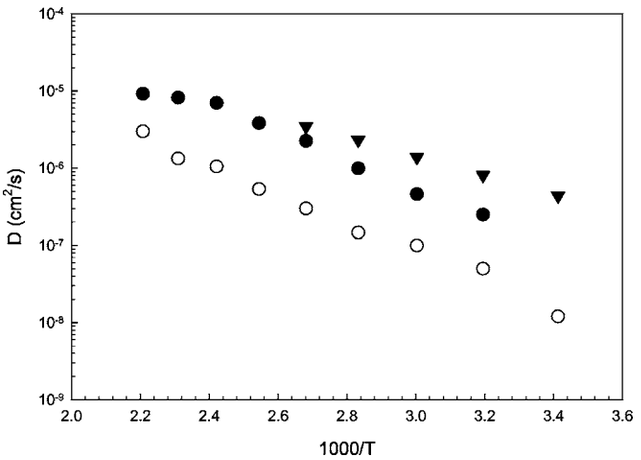

Figure 3. (Filled circle) Temperature dependence of the proton diffusion in *m*-PBI-ppa membranes. Measurements on 100% (inverted filled triangle) PA and (unfilled circle) PPA are included for comparison.

in diffusion activation energy appears to occur around 130°C in *m*-PBI-ppa, although there are too few data points to calculate a meaningful activation energy.

Arrhenius plots of ^{1}H T_1 and T_2 for dried *m*-PBI-imb and *m*-PBI-ppa are displayed in Fig. 4. Although the T_2 temperature dependences in the membranes are quite similar in appearance, the T_2 values for *m*-PBI-imb are considerably lower, accounting for the difficulties in measuring diffusion as described above. It is clear that the short-range interactions that govern spin–lattice relaxation differ

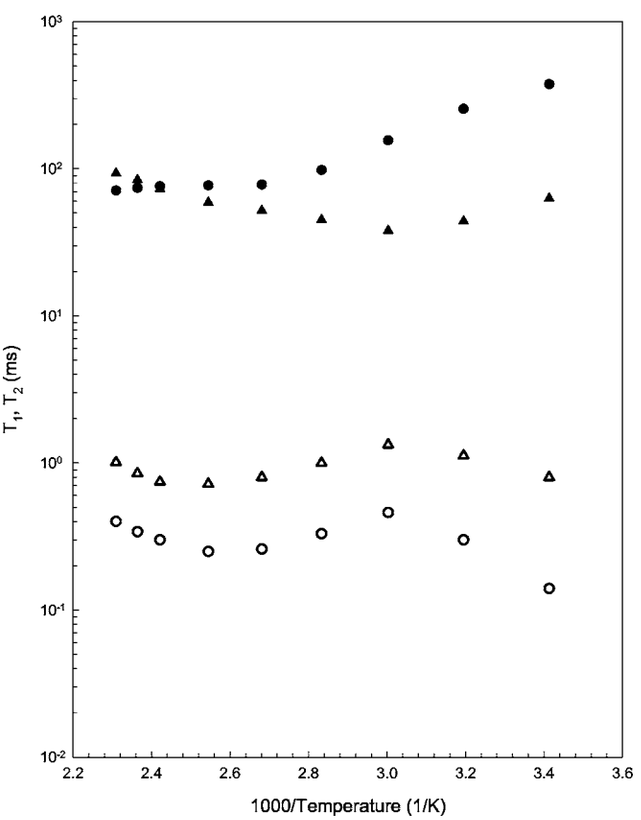

Figure 4. Arrhenius plot of (filled symbols) ^{1}H T_1 and (unfilled symbols) T_2 for (circles) *m*-PBI-imb and (triangles) *m*-PBI-ppa.

between the two materials. A broad T_1 minimum is observed in *m*-PBI-ppa. To the extent that the minimum can be ascertained in *m*-PBI-imb, it almost certainly occurs at higher temperatures, indicating that short-range proton mobility at a given temperature is higher in *m*-PBI-ppa. As the motional correlation time at the T_1 minimum is comparable to the reciprocal of the NMR angular frequency, the relaxation process is governed by short-range molecular motions such as rotations or intermolecular hops, which may ultimately be related to long-range transport, the latter clearly more facile in the *m*-PBI-ppa on the basis of the diffusion results. Apart from these observations it is notable that the spin–spin relaxation time T_2 dependence on temperature does not follow the most commonly observed situation of monotonic increase when passing from the rigid limit to the extreme narrowing regime but actually goes through a minimum, and that $T_2 \ll T_1$ in the vicinity of the T_1 minimum. Such anomalous relaxation time behavior has been observed to occur in systems[13-16] where there is highly correlated ion motion or reduced dimensionality in disordered systems. The disparity between T_1 and T_2 values is less for the *m*-PBI-ppa than for the *m*-PBI-imb sample, suggesting that such correlation or reduced dimensionality effects are more significant in the latter. It is speculated at this time that the somewhat lower acid content of *m*-PBI-imb relative to the *m*-PBI-ppa film, as well as the possible differences in the distribution of PA in the membranes caused by different morphologies, increases the likelihood of molecular-level interaction between the acid and host polymer, leading to a greater departure from uncorrelated isotropic ion transport expected for a homogeneous medium.

Phosphorus-31 spectra of PPA, *m*-PBI-imb, and *m*-PBI-ppa at 20 and 140°C are displayed in Fig. 5. The PPA spectrum exhibits three peaks, with the small one at the reference frequency indicating a relatively small amount of PA. The peak at about −14 ppm (~1.7 kHz) is assigned to the dimeric compound pyrophosphoric acid and the −30 ppm peak (~3.7 kHz) is attributed to the higher oligomeric species, within the range of spectral assignments for condensed phosphate compounds reported by Crutchfield et al.[17] Both membranes exhibit the PA resonance and, to a lesser extent, that of the dimer. The absence of the 30 ppm peak verifies that hydrolysis of the PPA phase into PA has occurred. The spectral components in *m*-PBI-imb are significantly broader than in *m*-PBI-ppa at 20°C, but exactly the reverse behavior is observed at elevated temperature (140°C). The difference in linewidths at low temperature is attributed to greater restriction of both translational and rotational phosphate group motion by the PBI matrix in the *m*-PBI-imb sample. This is believed to arise from two factors: (*i*) its lower PA/PBI ratio (Table I) and (*ii*) a greater degree of short-range intermixing of the PA with the PBI component in *m*-PBI-imb. The interesting reversal at high temperature, however, is attributed to exchange effects between the PA and dimer components, that is, the two components gradually merge into one broad line at 180°C (not shown). Transesterification in substituted phosphate and polyphosphate systems can occur in this system in a manner that is analogous to the transesterification reaction in carboxylic acid esters.[18] This interchange reaction can contribute significantly to the proton conduction mechanism, and the current results imply that this transformation occurs on a timescale comparable to the reciprocal of the spectral splitting (~2 kHz). Additional details regarding this point are discussed below. That this exchange phenomenon is not observed in *m*-PBI-imb could be the result of the above-mentioned lower PA/PBI ratio or the differences in PA distribution in the membrane resulting from the different processes used to prepare the membranes.

Diffusion results for ^{31}P, plotted in Fig. 6, are presented only for the three peaks of PPA and 100% PA because, as in the case of proton diffusion measurements in *m*-PBI-imb, the T_2 values were too short to acquire meaningful diffusive echo decays. Again, on the basis of measured T_2 values, and known gradient strengths, durations, and spacings, we therefore quote an upper limit of ~3 × 10^{-9} cm^2/s for phosphate diffusion in both of the membranes,

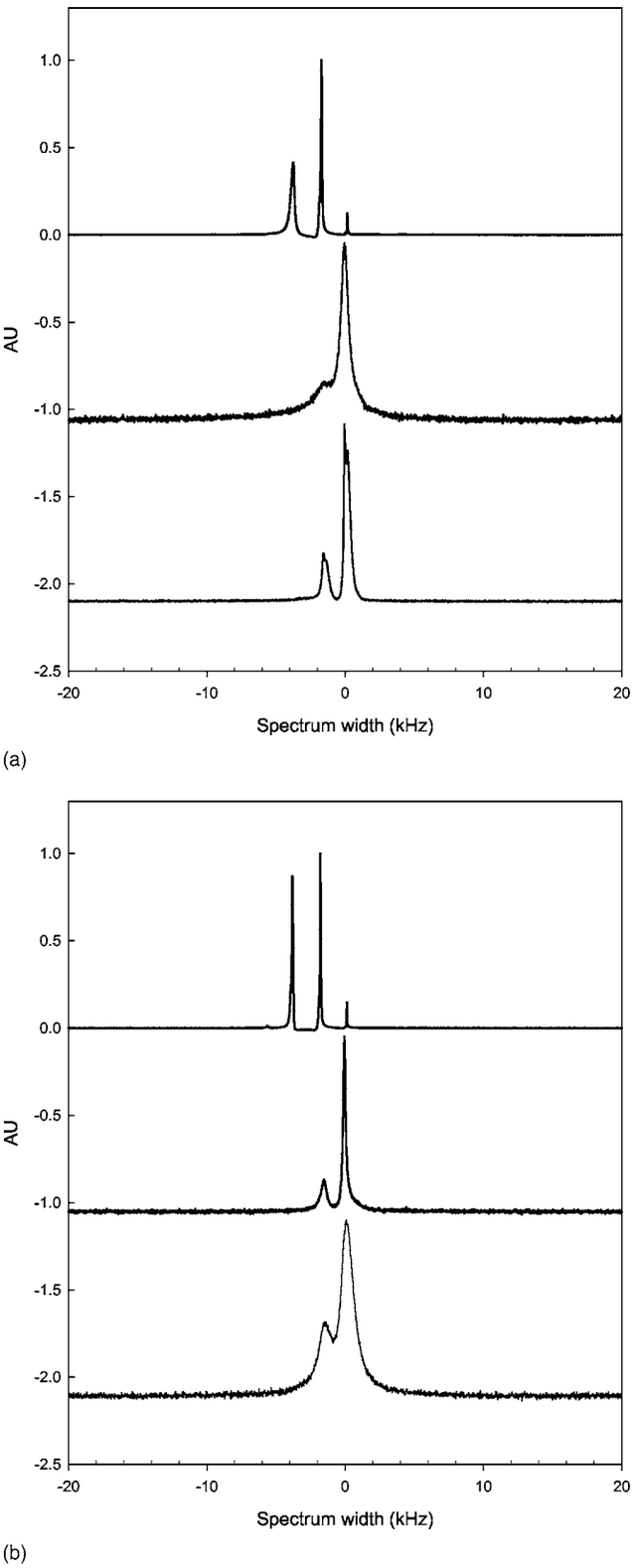

Figure 5. ^{31}P NMR spectra for (upper curve) PPA, (middle curve) *m*-PBI-imb, and (lower curve) *m*-PBI-ppa at (a) 20 and (b) 140°C.

approximately 2–3 orders of magnitude lower than the proton diffusion. Thus, it is clear that the membranes, at least *m*-PBI-ppa for which proton diffusion was directly measured, are essentially pure

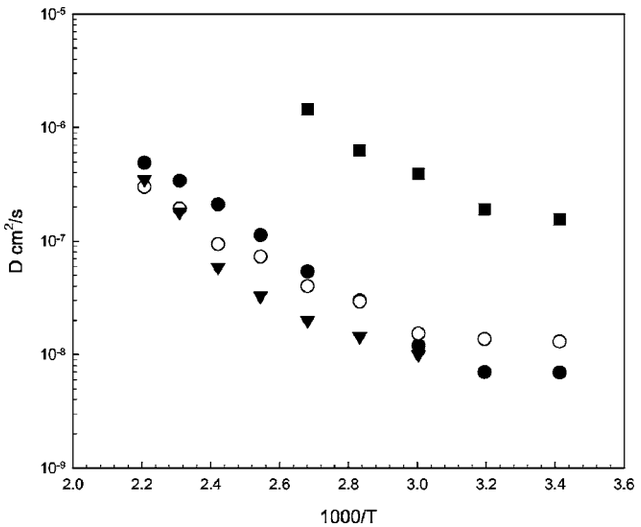

Figure 6. Arrhenius plot of ^{31}P diffusion for the (filled circles) PA, (open circles) PPA, and (inverted filled triangles) higher oligomeric peaks of PPA, and (filled squares) a separate sample of 100% PA.

proton conductors. As mentioned in the introduction, the phosphate diffusion in pure PA and in 85% PA is governed by a vehicular mechanism that depends on viscosity. The low phosphate diffusivity then implies a high effective viscosity, which is certainly expected for a membrane as opposed to liquid PA or PPA. The diffusion coefficients of the resolvable NMR peaks in PPA overlap considerably, implying cooperative motion. This is clear from the observation that the PA phase of the PPA is less mobile than in pure PA. Figure 7 displays Arrhenius plots of T_1 for the three resolvable species in PPA, 100% PA, and the PA-associated peak in *m*-PBI-ppa (no T_1 measurements were made in the *m*-PBI-imb sample). There is also significant overlap of the T_1 values among the resolvable ^{31}P components of the PPA, implying cooperative motion at a shorter timescale than the diffusion process. The T_1 values are quite low in the membrane, demonstrating a different local environment for the phosphate ions in the film compared to PA or PPA, but not low

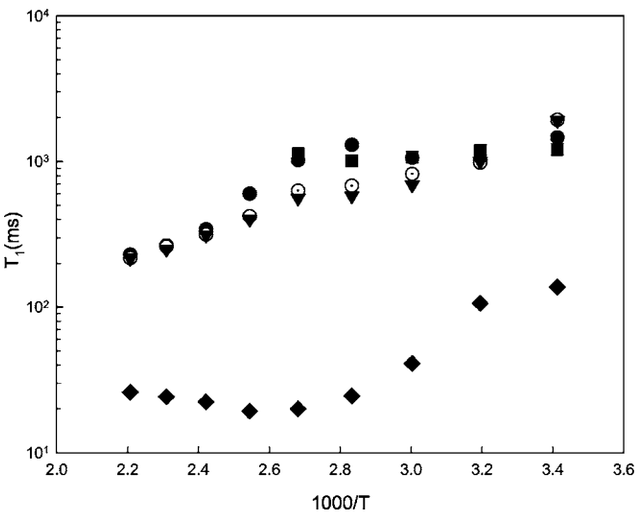

Figure 7. Arrhenius plot of the ^{31}P T_1 relaxation time for the (filled circles) PA, (open circles) PPA, and (inverted filled triangles) higher oligomeric peaks of PPA, (filled diamonds) *m*-PBI-ppa, and (filled squares) 100% PA.

enough to give a significant contribution to the high-temperature spectral broadening, therefore lending additional credence to the exchange hypothesis described above.

Conclusions

Proton transport in PA-doped *m*-PBI membranes fabricated by a conventional imbibing process and a novel sol-gel process were characterized by NMR methods. At similar PA loading levels, proton diffusivity is ascertained to be about an order of magnitude higher in the *m*-PBI-ppa membranes compared to those prepared by the conventional imbibing method, demonstrating the significant difference in membrane processing on transport properties. This is consistent with ionic conductivity measurements made on the bulk films. Phosphate counter-ion mobility was inferred to be more than 2 orders of magnitude lower that of the protons, which supports a Grotthus-type mechanism of proton conduction. The presence of short-range interactions between the anions and the polymer matrix is inferred from ^{31}P linewidth T_1 and T_2 measurements, which differ in values and temperature dependence from pure PA or PPA. There are also differences in ^{31}P NMR behavior observed between the two kinds of membranes, one being that short-range phosphate motion is more restricted in *m*-PBI-imb and the other involving an exchange phenomenon between molecules of PA and a pyrophosphate dimer, which is attributed to the higher concentration of PA in the PPA-processed films and the differences in PA distribution caused by variations in film morphology. It is suggested that this exchange mechanism could arise from a transesterification process and may provide a contribution to the overall proton conductivity.

Acknowledgments

The research at Hunter College was supported in part by the U.S. Air Force Office of Scientific Research and a National Institutes of Health RCMI Infrastructure grant (RR-03037). S.H.C. and L.D. are grateful for grant support from the Research Corporation, WPU Center for Research and A.R.T. This research was also partially supported by the U.S. Department of Energy (BES, DDE-FG02-OSER46258).

Hunter College of CUNY assisted in meeting the publication costs of this article.

References

1. P. Jannasch, *Curr. Opin. Colloid Interface Sci.*, **8**, 96 (2003).
2. R. Savinell, E. Yeager, D. Tryk, U. Landau, J. Wainright, D. Weng, K. Lux, M. Litt, and C. A. Rogers, *J. Electrochem. Soc.*, **141**, L46 (1994).
3. J. S. Wainright, J.-T. Wang, D. Weng, R. F. Savinell, and M. Litt, *J. Electrochem. Soc.*, **142**, L121 (1995).
4. D. Weng, J. S. Wainright, U. Landau, and R. F. Savinell, in *Proton Conducting Membrane Fuel Cells I*, S. Gottesfeld, G. Halpert, and A. Landgrebe, Editors, PV 95-23, p. 214, The Electrochemical Society Proceedings Series, Pennington, NJ (1995).
5. J.-T. Wang, R. F. Savinell, J. Wainright, M. Litt, and H. Yu, *Electrochim. Acta*, **41**, 193 (1996).
6. L. Xiao, H. Zhang, E. Scanlon, L. S. Ramanathan, E.-W. Choe, D. Rogers, T. Apple, and B. C. Benicewicz, *Chem. Mater.*, **17**, 5328 (2005).
7. L. Xiao, H. Zhang, T. Jana, E. Scanlon, R. Chen, E.-W. Choe, L. S. Ramanathan, S. Yu, and B. C. Benicewicz, *Fuel Cells*, **5**, 287 (2005).
8. S. H. Chung, S. Bajue, and S. G. Greenbaum, *J. Chem. Phys.*, **112**, 8515 (2000).
9. S. H. Chung, Y. Wang, W. Bzucha, G. Zukowska, S. G. Greenbaum, and W. Wieczorek, *Electrochim. Acta*, **46**, 1651 (2001).
10. K. A. Mauritz and R. B. Moore, *Chem. Rev. (Washington, D.C.)*, **104**, 4535 (2004).
11. T. A. Zawodzinski, Jr., C. Derouin, S. Radzinski, R. J. Sherman, V. T. Smith, T. E. Springer, and S. Gottesfeld, *J. Electrochem. Soc.*, **140**, 1041 (1993).
12. J. R. P. Jayakody, P. E. Stallworth, E. S. Mananga, J. Farrington-Zapata, and S. G. Greenbaum, *J. Phys. Chem. B*, **108**, 4260 (2004).
13. S. W. Martin, H. J. Bishoff, M. Mali, J. Roos, and D. Brinkmann, *Solid State Ionics*, **18/19**, 421 (1986).
14. P. M. Richards, *in Physics of Superionic Conductors*, M. B. Salamon, Editor, p. 141, Springer, Berlin (1979).
15. J. L. Bjorkstam and M. Villa, *Phys. Rev. B*, **22**, 5025 (1980).
16. P. A. Beckmann, *Phys. Rep.*, **171**, 85 (1988).
17. M. M. Crutchfield, C. F. Callis, R. R. Irani, and G. C. Roth, *Inorg. Chem.*, **1**, 813 (1962).
18. D. E. C. Corbridge, *Phosphorus, An Outline of Its Chemistry, Biochemistry, and Technology*, 4th ed., Elsevier, New York (1990).